A Simple RVoG Test for PolInSAR Data

J. David Ballester-Berman, Fernando Vicente-Guijalba, and Juan M. Lopez-Sanchez, *Senior Member, IEEE*

***Abstract*—In this paper, we present a simple algorithm for assessing the validity of the RVoG model for PolInSAR-based inversion techniques. This approach makes use of two important features characterizing a homogeneous random volume over a ground surface, i.e., the independence on polarization states of wave propagation through the volume and the structure of the polarimetric interferometric coherency matrix. These two features have led to two different methods proposed in the literature for retrieving the topographic phase within natural covers, i.e., the well-known line fitting procedure and the observation of the (1, 2) element of the polarimetric interferometric coherency matrix. We show that differences between outputs from both approaches can be interpreted in terms of the PolInSAR modeling based on the Freeman-Durden concept, and this leads to the definition of a RVoG/non-RVoG test. The algorithm is tested with both indoor and airborne data over agricultural and tropical forest areas.**

***Index Terms*—Parameter inversion, PolInSAR, RVoG model, vegetation.**

I. Introduction

THE ESTIMATION of vegetation structural parameters by means of polarimetric SAR interferometry (PolInSAR)-based techniques stems from a few key contributions that still remain as the basis of the PolInSAR paradigm. These contributions were the development of the random volume over ground (RVoG) model by Treuhaft *et al.* [1]–[3] and the concept itself of PolInSAR [4]–[6], originally proposed by Cloude and Papathanassiou in 1998.

Experimental validation of PolInSAR techniques has been successfully carried out over forest areas in terms of forest height and/or forest biomass [7]–[13] and as well as 3-D scattering profiles by means of tomographic processing [14]–[16]. Indeed, 3-D tomographic processing merged with the polarimetric interferometric information arranged in the covariance matrix as a combination of Kronecker products has revealed that most of the PolInSAR-derived information is mapped as a result of the addition of two scattering mechanisms associated with ground and volume, respectively [17]–[19]. To this aim, airborne sensors have been widely used, as in the cited contributions, but only satellite missions such as TanDEM-X, and future TanDEM-L and BIOMASS (P-band sensor) will offer operational capabilities for global scale forest monitoring.

Manuscript received July 04, 2014; revised October 14, 2014; accepted November 26, 2014. This work was supported by the Spanish Ministry of Economy and Competitiveness (MINECO) and EU FEDER under Project TEC2011-28201-C02-02.

The authors are with the Signals, Systems and Telecommunication Group and the Institute for Computing Research (IUII), University of Alicante, Alicante 03080, Spain (e-mail: davidb@ua.es).

Color versions of one or more of the figures in this paper are available online at http://ieeexplore.ieee.org.

Digital Object Identifier 10.1109/JSTARS.2014.2379438

Also some interest has been focused on the potential of PolInSAR observables for agriculture monitoring. Although the morphology of such a vegetation type is totally different to forests, some works have studied the possibilities for adapting the existing framework for forest monitoring to estimate agriculture parameters [20]–[23]. In [21] and [22], a first experimental validation under laboratory conditions for maize and rice samples and a wide range of frequencies were presented, and in [23], it was shown that under certain circumstances, reliable height estimates from maize and winter rape fields are also feasible with airborne data using the RVoG.

All current monitoring techniques considering the PolInSAR concept rely on the fact that the number of observables and parameters must be balanced. As a consequence, physical models employed for inversion purposes must observe a tradeoff between complexity and practical utility. This is the reason that makes the RVoG [1], [3] a perfect candidate to be used for quantitative and qualitative vegetation monitoring. Actually, this advantageous feature arises as a consequence of the first-order approximation of the electromagnetic response for targets within vegetated scenarios. This model assumes that scattering properties of the target are characterized by three mechanisms corresponding to direct surface, dihedral-type, and a random volume. In fact, this constitutes the model proposed by Freeman and Durden for polarimetric SAR (PolSAR) data [24], [25] which has become the basis for many PolSAR-based monitoring techniques. Actually, a number of works arisen in recent years [26]–[32] have contributed to improve the original concept by Freeman and Durden. The reader is referred to [33] for a more detailed vision of such a topic. Additionally, the PolSAR decomposition case has also been extended to versions focused on PolInSAR observables [11], [34] which have shown some evidences on their potential to contribute to a more accurate estimation of vegetation structural parameters.

Therefore, it becomes evident that current (and future) strategies for PolInSAR data exploitation must be devised as simple as possible in order to define practical approaches and invertible electromagnetic models. Indeed, one particular feature that contributes to this aim is the modeling of vegetation as a random volume since it entails a reduction of the number of parameters with respect to other models such as the oriented volume or a hybrid version considering both isotropic and anisotropic propagations through a layered medium.

In this regard, and considering that the concept of "random volume" plays a key role in PolInSAR techniques, it is necessary to have at disposal a tool to check the validity of the RVoG model before being applied for information retrieval.

One existing strategy to deal with this issue consists of assessing the RVoG model fitting by testing one of the assumptions of the model, i.e., the equiscattering mechanisms (ESM)

assumption. One way to implement such an approach is by means of the maximum likelihood ratio of the coherency matrices, as proposed in [35]. Some limitations of such a strategy arise as a consequence of its dependence on the total backscattering level. Therefore, an alternative approach considering the detection of polarimetric features, i.e., a polarimetric change detector [36], has been introduced and modified in order to perform the ESM test [37], [38]. An alternative methodology was recently developed in [39]. In that work, authors perform an in-depth analysis of the RVoG hypothesis and define the maximum likelihood estimator of the PolInSAR coherency matrix. Then, they derive the generalized likelihood ratio test of the RVoG model.

Alternatively, in this paper, we propose a simpler approach to check the RVoG assumption. This is based on two well-known features commonly used within the PolInSAR framework, i.e., the independence on polarization states of wave propagation through the random volume and the structure of the polarimetric interferometric coherency matrix. The first one was exploited to derive the *line fitting* procedure that enables the underlying topography estimation on a vegetated area [6]. The second one was used in [40] to derive a closed expression of the topographic phase assuming that the vegetated area fulfills the RVoG assumption. On the basis of the RVoG scenario, both approaches should yield similar topography estimates. Otherwise, potential differences, which must be assessed by means of histogram analysis, will be interpreted as the nonvalidity of the RVoG assumption. We will show that this interpretation is supported in terms of Freeman–Durden decomposition concept applied to PolInSAR [34].

Concerning the RVoG parameter estimation, it is noted that an early approach based on a maximum likelihood analysis of different scenarios, i.e., bare surface, random volume, and RVoG, was proposed in [41]. These inversions include full polarimetric covariance matrix estimates as well as values for structural parameters (canopy height, bare earth topography, and extinction) that maximize the log likelihood of the input coherency matrix. This is a rigorous treatment of the inversion problem, and it potentially could contribute to improve the estimation accuracy of model parameters. Nevertheless, validation and/or comparison with other parameter estimation methods, in particular with the line fitting approach remains a pending task.

The paper is organized as follows. In Section II, a short review on some PolInSAR concepts is given. Section III describes the algorithm proposed, and its performance is analyzed. Finally, Section IV draws the main conclusion of the paper.

II. Some Concepts on PolInSAR Modeling

According to the previous comments, we make use of two main features of the RVoG for defining the test proposed in this paper. The first one has to do with the isotropic propagation of the wave characterizing a random volume. It has important implications for parameter retrieval by PolInSAR since it led to the observation [6] that the coherences are arranged as a line on the complex plane. This enabled the development of the *line fitting* procedure for estimation of the underlying topography on a vegetated area [6] and, subsequently, the estimation of other vegetation parameters such as volume height and extinction. This strategy was later adapted and tested for agricultural vegetation [21] where the oriented volume hypothesis, i.e., anisotropic propagation [2], should theoretically replace the random volume. Actually, it was shown that the line arrangement of coherences was undermined in the agricultural case with regard to forest scenarios. However, the impact of these anisotropic effects is not so important and the conclusion so far is that the RVoG can be even applied for agricultural areas under certain conditions [23]. These conditions are basically a minimum dynamic range on the ground-to-volume ratios, and an appropriate design of the interferometer (vertical wavenumber) to deal with both sensitivity and volume decorrelation issues. Note that these issues were theoretically studied in [42] and [43] for different interferometric configurations and ground contributions.

The second feature has to do with the structure of the polarimetric interferometric coherency matrix. This idea was used in [40] to derive a closed expression of the topographic phase assuming that the vegetated area fulfills the RVoG assumption. In [40], authors resorted to the known matrix structure of a RVoG and pointed out that the (1,2) entry of the Ω_{12} matrix is made up by contributions (both interferometric and polarimetric) originated at the ground. In order to retrieve the topographic phase from the interferometric part, the polarimetric contribution to the phase is first removed by exploiting the polarimetric information. This leads to expression (1), where T is the PolSAR coherency matrix. This particular expression was subsequently shown to be a particular solution of the general approach proposed in [44]

$$\phi_0 = \arg(\Omega_{12}(1,2) \cdot \mathrm{T}(2,1)). \tag{1}$$

For a RVoG scene, the line fitting and (1) approaches should yield very close estimates, so any disagreement between them can be justified as a violation of the RVoG hypothesis. To support this statement, we resort to a previous work [34] where Freeman–Durden concept is extended to PolInSAR observations. We consider the three scattering mechanisms corresponding to direct surface, dihedral-type and a random volume, as proposed by Freeman and Durden, and different wave paths induced by interferometric observations in order to model the elements of the interferometric cross-correlation matrix formed in the lexicographic basis, i.e., $\mathbf{C_{12}} = \mathbf{C_{vol}} + \mathbf{C_{dbl}} + \mathbf{C_{odd}}$. This procedure leads to the following decomposition for each entry (assuming reflection symmetry):

$$\begin{aligned}
C_{12}(1,1) &= F_v + F_d + F_s \\
C_{12}(1,3) &= \alpha F_d + \beta F_s + \frac{F_v}{3} \\
C_{12}(2,2) &= \frac{2}{3} F_v \\
C_{12}(3,1) &= \alpha^* F_d + \beta^* F_s + \frac{F_v}{3} \\
C_{12}(3,3) &= |\alpha|^2 F_d + |\beta|^2 F_s + F_v
\end{aligned} \tag{2}$$

where there are five complex unknowns. Among them, F_v, F_d, F_s account for the complex cross-correlation amplitudes

of volume, double-bounce and direct scattering, respectively, whereas α and β are defined in terms of Fresnel and Bragg coefficients [25].

As proposed by Freeman and Durden, we assume in the interferometric case that the $\mathbf{C_{12}}(2,2)$ element comes only from the volume contribution. Consequently, after estimating the volume contribution, the remaining matrix $\mathbf{C_r}$ is expressed as

$$\begin{aligned}\mathbf{C_r} &= \mathbf{C_{dbl}} + \mathbf{C_{odd}} \\ &= \begin{bmatrix} F_d + F_s & 0 & \alpha F_d + \beta F_s \\ 0 & 0 & 0 \\ \alpha^* F_d + \beta^* F_s & 0 & |\alpha|^2 F_d + |\beta|^2 F_s \end{bmatrix}\end{aligned} \tag{3}$$

where the $\mathbf{C_r}$ matrix has four complex unknowns, and it leads to a determined nonlinear equation system which can be solved numerically.

Some issues regarding both the definition of the model and the numerical optimization used for solving the problem in (3) are discussed in [45]. Nevertheless, it is pointed out that the construction of model (2) is consistent with other studies within the PolInSAR paradigm since they all share the same principle regarding the addition of uncorrelated contributions of first-order scattering mechanisms. Therefore, we will use this model to interpret possible differences between the line fitting and (1) approaches in order to decide whether a vegetated area corresponds to either a random or a nonrandom volume over ground in a straightforward manner.

For this purpose, first we will get the corresponding cross-correlation matrix in the Pauli basis $\mathbf{\Omega_{12}}$ from the lexicographic one of the model defined in (2) by means of the unitary transformation in (4)

$$\mathbf{\Omega_{12}} = \mathbf{A}^{*T}\mathbf{C_{12}}\mathbf{A} \tag{4}$$

wherein

$$\mathbf{A} = \frac{1}{\sqrt{2}}\begin{bmatrix} 1 & 1 & 0 \\ 0 & 0 & \sqrt{2} \\ 1 & -1 & 0 \end{bmatrix}. \tag{5}$$

Therefore, the term $\Omega_{12}(1,2)$ is defined as

$$\begin{aligned}\Omega_{12}(1,2) = 1/2 \cdot \big[&F_s \cdot (1 - j2\Im(\beta) - |\beta|^2) \\ &+ F_d \cdot (1 - j2\Im(\alpha) - |\alpha|^2)\big]\end{aligned} \tag{6}$$

where $F_s = |F_s| \cdot e^{j\cdot\phi_s}$ and $F_d = |F_d| \cdot e^{j\cdot\phi_d}$. The term ϕ_s corresponds to the interferometric phase for the direct scattering, whereas the phase of double-bounce mechanism F_d is assumed at the ground level, i.e., $\phi_d = \phi_0$.

Expression (6) can be formulated in a compact way by introducing the complex numbers k_β and k_α accounting for expressions depending upon β and α, respectively. Then

$$\Omega_{12}(1,2) = F_s \cdot k_\beta + F_d \cdot k_\alpha \tag{7}$$

where the $1/2$ factor is included in k_β and k_α. Now, if we consider the original Freeman–Durden decomposition for PolSAR data, the (2,1) term of the associated coherency matrix is given by

$$\begin{aligned}T(2,1) = 1/2 \cdot \big[&F_s^{pol} \cdot (1 + j2\Im(\beta) - |\beta|^2) \\ &+ F_d^{pol} \cdot (1 + j2\Im(\alpha) - |\alpha|^2)\big]\end{aligned} \tag{8}$$

where the terms F_s^{pol} and F_d^{pol} are scattering intensities (real values) for direct and double-bounce mechanisms. Therefore, the element $T(2,1)$ can be written as

$$T(2,1) = F_s^{pol} \cdot k_\beta^* + F_d^{pol} \cdot k_\alpha^*. \tag{9}$$

Taking expressions (7) and (9) and computing the product shown in (1) [40] leads to expression given in (10) as

$$\begin{aligned}&\Omega_{12}(1,2) \cdot T(2,1) \\ &\quad= \Big[|F_s| \cdot F_s^{pol} \cdot |k_\beta|^2 + |F_s| \cdot F_d^{pol} \cdot k_\beta \cdot k_\alpha^*\Big] \cdot e^{j\cdot\phi_s} \\ &\qquad+ \Big[|F_d| \cdot F_s^{pol} \cdot k_\alpha \cdot k_\beta^* + |F_d| \cdot F_d^{pol} \cdot |k_\alpha|^2\Big] \cdot e^{j\cdot\phi_0}.\end{aligned} \tag{10}$$

Assuming that backscattering amplitudes F_s^{pol} and F_d^{pol} are equal to $|F_s|$ and $|F_d|$, respectively, then expression (10) becomes

$$\begin{aligned}&\Omega_{12}(1,2) \cdot T(2,1) \\ &\quad= \big[|F_s|^2 \cdot |k_\beta|^2 + |F_s| \cdot |F_d| \cdot k_\beta \cdot k_\alpha^*\big] \cdot e^{j\cdot\phi_s} \\ &\qquad+ \big[|F_d| \cdot |F_s| \cdot k_\alpha \cdot k_\beta^* + |F_d|^2 \cdot |k_\alpha|^2\big] \cdot e^{j\cdot\phi_0}.\end{aligned} \tag{11}$$

In general, expression (11) contains both intensity and phase terms corresponding to direct and double-bounce mechanisms. As seen, both terms in the summation contain polarimetric phase contributions accounted for by terms $k_\beta \cdot k_\alpha^*$ and $k_\alpha \cdot k_\beta^*$, respectively. On the other hand, the interferometric phase appears as ϕ_s for the direct scattering and ϕ_0 for the double-bounce. Therefore, we can conclude that whenever direct scattering is located at the ground interface the direct topography estimation by exploiting the matrix structure predicted by the RVoG model is valid. This is so because in such a case expression (11) turns into (12)

$$\begin{aligned}\Omega_{12}(1,2) \cdot T(2,1) = \big[&|F_s|^2 \cdot |k_\beta|^2 + 2 \cdot |F_s| \cdot |F_d| \cdot \Re(k_\beta \cdot k_\alpha^*) \\ &+ |F_d|^2 \cdot |k_\alpha|^2\big] \cdot e^{j\cdot\phi_0}.\end{aligned} \tag{12}$$

Therefore, from (12) the phase ϕ_0 can be directly retrieved as it was proposed in [40].

On the other hand, i.e., in case that $\phi_s \neq \phi_0$, it is interpreted as the vegetation layer contains some oriented structures (either horizontal or vertical) above the ground level, or alternatively, as some other effects are not well modeled. Consequently, it will break down the homogeneous random volume distribution of scatterers. As a result, it will induce additional phase terms that will prevent the direct estimation of topography from (1) and in addition, the arrangement of coherences as a line would not be possible. In spite of this potential modeling error, some previous works in the literature have shown that the line fitting approach has a great robustness to minimize both residual speckle and orientations effects that could affect the data. Actually, it has been demonstrated not only for agricultural areas [21] but also for forests at P-band where potential orientation effects could affect the observations [9]. In any case, it must be noted that it could be possible that the two methods could give the same wrong ground estimates even when the RVoG model is not valid. In such a case, the approach proposed here would fail.

As shown in Section III, the utility of these observations is twofold: 1) they will be useful for explaining the differences found between the two topography estimation methods, and consequently; 2) they enable the formulation of a simple algorithm to discriminate between randomly and nonrandomly oriented volumes over ground surface.

III. Algorithm and RVoG Test Validation

According to the previous analysis, the proposed approach consists of first estimating the topographic phase for each pixel within the scene by means of both the line fitting [6] and expression in (1) [40]. Then, by comparing both estimates we will conclude that the RVoG is a suitable model whenever the topography values are similar. Contrarily, one must expect nonmodeled effects in the wave propagation path and this fact should also be taken into account for parameter inversion. For a practical implementation of such an algorithm a threshold to decide whether the phase (or height) difference between both methods is low enough (or not) must be set. If their difference is lower than or equal to the proposed threshold then the RVoG assumption is fulfilled. Fig. 1 shows the flowchart of the algorithm. A plausible criterion is to set this threshold as a function of the volume height, which should be *a priori* known or estimated. However, since volume height is usually unknown this criterion is not valid. This point will be later discussed in the experimental analysis.

Next, the performance of the proposed algorithm is tested by using three different data sets: 1) an indoor data set from a maize sample from S- to X-band [16], [21] acquired at the EMSL, JRC-Ispra (Italy); 2) an airborne data set at L-band acquired during the AgriSAR 2006 campaign by DLR's E-SAR sensor over a variety of agricultural crops [46]; and 3) a P-band data set over tropical forest gathered by DLR's E-SAR system during the INDREX-II campaign [9].

A. Indoor data

PolInSAR data on a maize sample were acquired from S- to X-band and the vegetation volume was 1.8 m high. The actual ground topographic height of the maize sample is $-0.88\,\mathrm{m}$, since the ground is 0.38 m below the EMSL focus and the images were focused 0.5 m above it (see [21] for more details). Fig. 2 shows the topographic phase estimates from the classical line fitting algorithm, the method from (1), and the actual topography for comparison purposes, where 51 frequency points uniformly distributed between 2 and 9 GHz were taken, i.e., steps of 140 MHz. The corresponding topographic heights can be obtained from the relationship $h = \phi/k_z$. In general, it is clear that the line fitting procedure performs better; however, it can be said that both methods yield similar estimates only up to about 5 GHz. There is an evident departure of both methods from the actual topography within the 5–6 GHz range. Also, from 6 to 8 GHz the line fitting performs perfectly whereas the method from (1) does not yield right values. Fig. 3 displays the absolute value of the topographic phase difference between both methods.

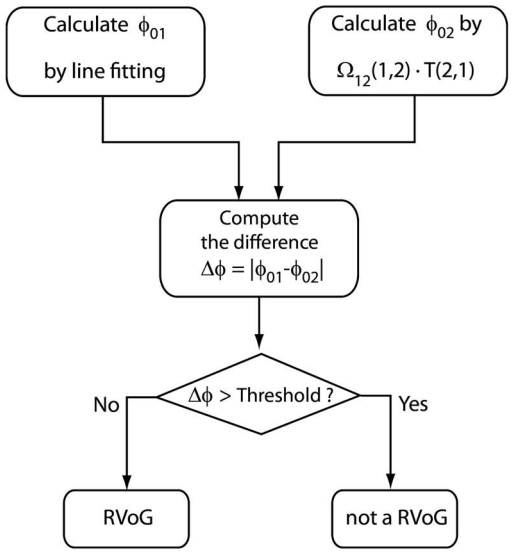

Fig. 1. Flowchart of the proposed algorithm for the RVoG test.

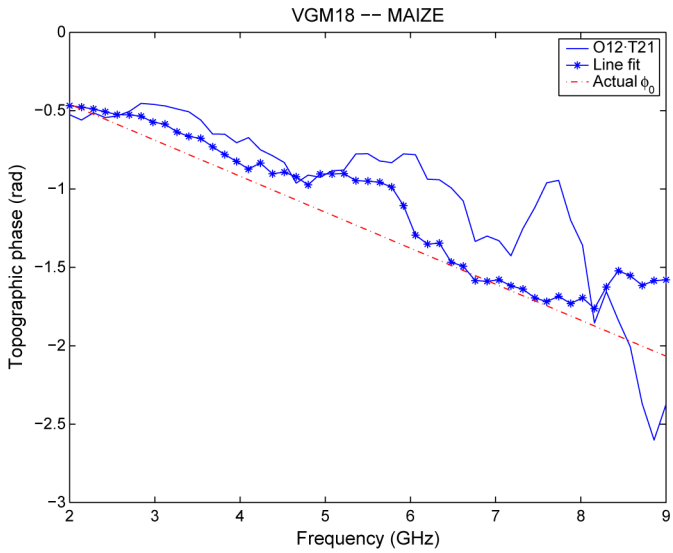

Fig. 2. Topographic phase estimates for the EMSL maize sample as a function of frequency: (solid) (1), (stars) line fit, and (dashed–dotted) actual value.

Disagreements between both methods can be explained because of different robustness of each retrieval strategy. As shown in [21], the line fitting approach is robust enough to provide correct topography estimates up to 8 GHz. In other words, this method is able to minimize propagation effects that are not considered in the RVoG definition and correct estimates are still possible. On the contrary, it was also shown that as frequency increases the volume decorrelation becomes stronger and, consequently, the coherences are not arranged in a line any more, i.e., the wave propagation through the canopy is not polarization-independent. Additionally, it is also noted that another effect that breaks down the RVoG validity at higher frequencies is the relatively larger dimensions of particles in the volume with respective to wavelength which causes the approximation of small random scatterers to fail. This aforementioned behavior affects more directly the correlation between the first and second Pauli channels and, consequently,

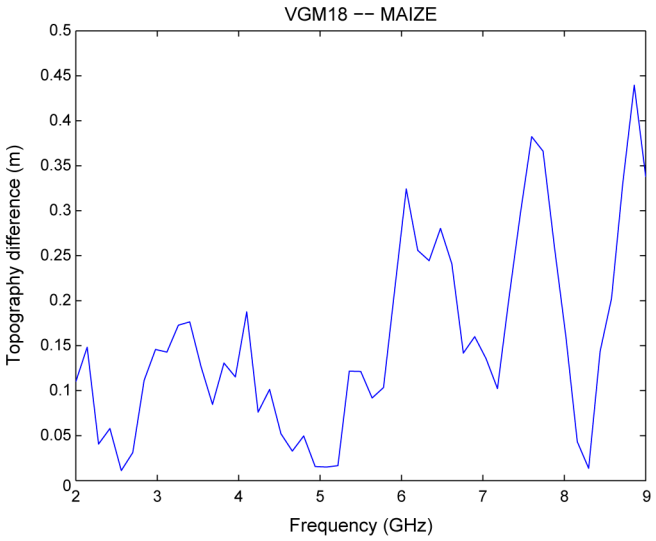

Fig. 3. Absolute value of the topographic phase difference between both methods for the EMSL maize sample as a function of frequency.

the phase $\arg(\Omega_{12}(1,2)T(2,1))$ gets modified accordingly by those volume contributions.

It is emphasized that these conclusions were also in agreement with the outputs of the tomographic analysis by means of the PCT (Polarization Coherence Tomography) [16] where the vertical scattering profiles suggested that the vertical polarization response is dominated by the volume contribution, without echoes from the ground, specially from 6 GHz.

As it will be shown in Section III-B1, the interpretation elaborated above is consistent with the results obtained for L-band data over a maize field, where the RVoG assumption seems to be partially fulfilled at this low frequency.

For practical implementation of the proposed RVoG test, the threshold value for RVoG/non-RVoG discrimination remains to be decided. According to the results reported in previous works on topography estimation and its magnitude error [6], [21], [44], [47], a realistic value for this threshold value is 10%–15% of the volume height. By doing this, a 18–27 cm threshold would correspond to a 1.8-m high volume, whereas a 2.5–3.75-m limit would be used for a 25-m tall forest. According to this criterion, one could state that this vegetation sample behaves as an RVoG up to 6 GHz. For higher frequencies, there appear additional propagation effects that are not well modeled by a random volume. Notwithstanding the aforementioned criterion for setting the threshold, it must be noted that in most real situations the volume height is not known. Therefore, a different strategy for deciding the threshold value must be used. In the following, histograms will be used for such a purpose.

B. Airborne data

1) Agriculture: AgriSAR 2006 was an ESA funded campaign where 16 institutions were involved. During this campaign, a PolInSAR data set was also acquired by DLR on July 5, 2006 (i.e., DoY 186), and this will be employed in this paper. According to the available ground-truth from these campaigns,

Fig. 4. RGB image of the Agrisar 2006 test site. R = HH, G = HV, B = VV.

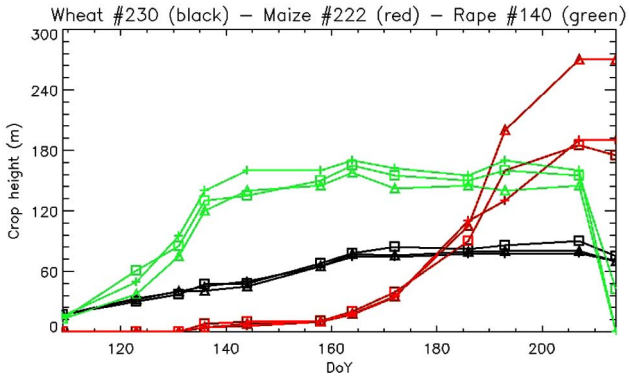

Fig. 5. Ground-truth measurements: Crop height evolution for (green) rape, (red) maize, and (black) wheat for the Agrisar 2006 test site at three measurement points.

this test site features a very flat area and very small topographic variations [46], which ranges between 0 m at far-range to about 40 m AMSL at near-range. Fig. 4 displays an RGB image of the study area for illustration purposes. Note that both maize and rape fields do not exhibit too much variability and there is a similar contribution of all three channels according to their grayish tone, even though it seems that the HH channel is the highest one. On the other hand, the VV and HH channels clearly dominate the response within wheat fields. Figure 5 plots the time evolution of height measurements taken from maize, wheat, and rape fields which are the crops on which we will focus our analysis.

According to the work in [23] where the same data set was used, the RVoG was successfully applied for topography and volume height estimation on rape and maize fields and, on the other hand, it failed to provide right estimates on wheat fields (see [46] for more details of the campaign). Besides, in order to support the later discussion on the results, we also reproduce the results on the retrieved vegetation height for rape, maize, and wheat, which were published in [23], as a way to provide a qualitative explanation for the differences shown in all three crops. These results are displayed in Table I. As shown, the retrieved

TABLE I
CROP HEIGHT ESTIMATES AT FIELD LEVEL AND GROUND-TRUTH FOR AGRISAR 2006 TEST SITE ON JULY 5, 2006 (DOY 186)

Field	Mean (m)	Std. dev. (m)	Ground data (m)
Rape 101	1.61	0.22	1.70, 1.72, 1.75
Rape 110	1.60	0.24	N.A.
Rape 130	1.67	0.25	N.A.
Rape 140	1.76	0.20	1.45, 1.50, 1.55
Maize 222	0.98	0.31	0.90, 1.05, 1.10
Wheat 230	1.06	0.33	0.77, 0.79, 0.82
Wheat 250	1.31	0.47	0.78, 0.80, 0.87

heights for rape are quite accurate with a low standard deviation. In case of maize, the mean height is also well estimated although the standard deviation is slightly higher than the rape case. Finally, there exist differences between the two fields of wheat, i.e., 230 and 250, where the latter exhibits a clear overestimation and high standard deviation. It is highlighted that these height estimates were computed using as input the topographic phase which was previously calculated by means of the line fitting approach. Consequently, the crop height values are a sort of indirect quality measure of the topography estimates.

Fig. 6 shows topography maps computed with both methods and Fig. 7 displays a map with the topography difference. Near- and far-range are the left and right sides of the map, respectively. Note the high variability at near-range in rape and maize which is caused by noisy interferometric phase within these areas.

The general impression is that phase differences are around zero for maize and rape fields, being more homogeneous in case of rape, whereas for wheat the values are different depending on the parcel considered. In order to confirm these qualitative observations, we have computed the histograms corresponding to the areas inside the light blue boxes in Fig. 6. Histograms for maize, rape, and wheat fields are plotted in Figs. 8–10, respectively.

As seen in the histograms, the difference between topography estimates for maize and wheat fields exhibits a bias whereas in case of rape fields the mean is zero. These results suggest that there exist some features in maize and wheat crops, so the RVoG assumption is not fulfilled. On the contrary, the rape fields are more homogeneous and the morphology of such a vegetation satisfies the RVoG. This is also in agreement with the impression from an *in situ* visual inspection of the fields as displayed in Fig. 11. On one hand, the rape plant structure is more uniform, whereas the expected oriented morphology for maize and wheat (primarily made up by the vertical stems) is disturbed by the other plant particles. These are the leaves, whose orientation and dimensions change as a function of plant height, and also the grains at the top of the volume in case of wheat crops. These structures can be regarded as a heterogeneous volume and they could be formulated in terms of two components, i.e., random plus oriented volumes, where both isotropic and anisotropic effects are induced [48]. It must be noted that in this particular data set the ground-truth campaign reports quite homogenous heights for all three crops (see Table I) for the acquisition date. However, the plant growth rate varies at parcel level and it depends also on the crop, as shown in Fig. 5. Note that 1 week later (July 12, 2006 which corresponds to DoY 193) the wheat crop growth remains very uniform within the same parcel. On the contrary, the rape crop exhibits some variations, whereas it is the maize crop for which the highest differences in height were found inside the same parcel.

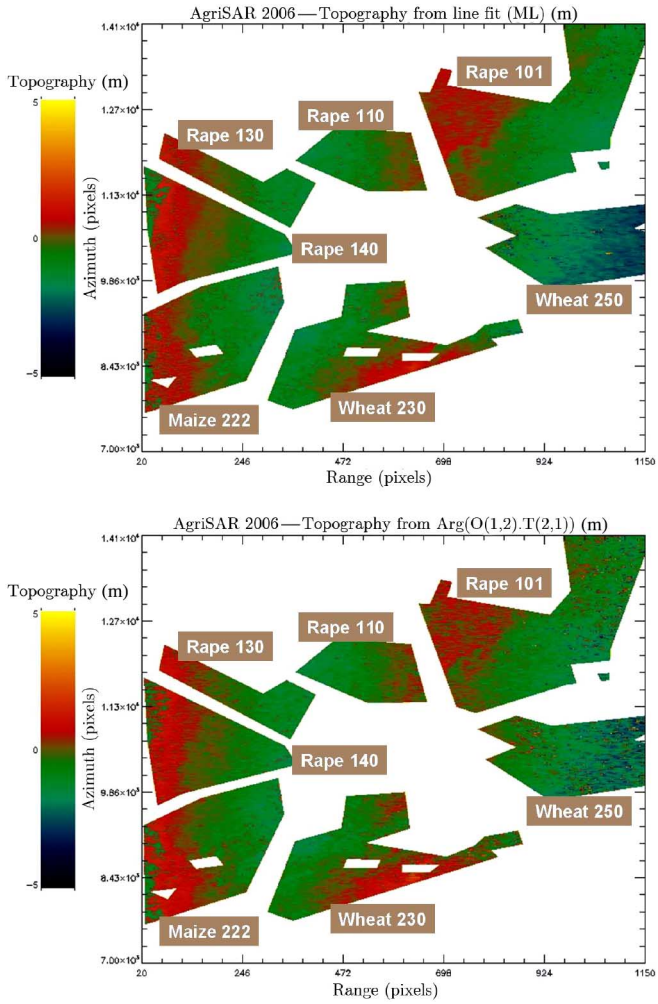

Fig. 6. Topographic height from both methods for the Agrisar 2006 test site. Top: line fit. Bottom: argument of product of matrix entries.

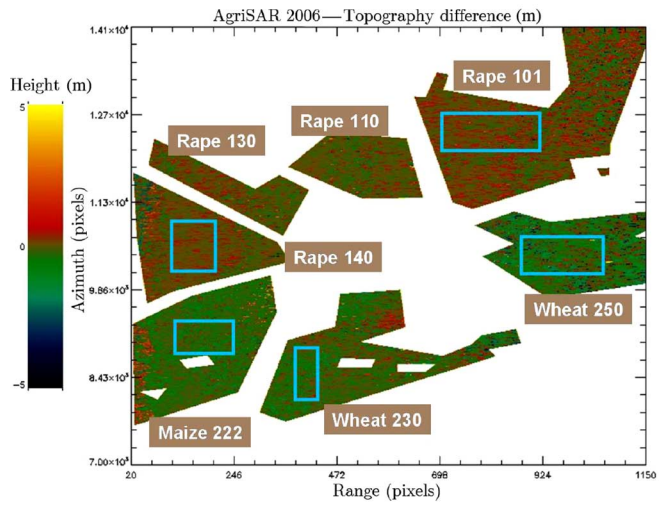

Fig. 7. Topography difference between both methods for the Agrisar 2006 test site.

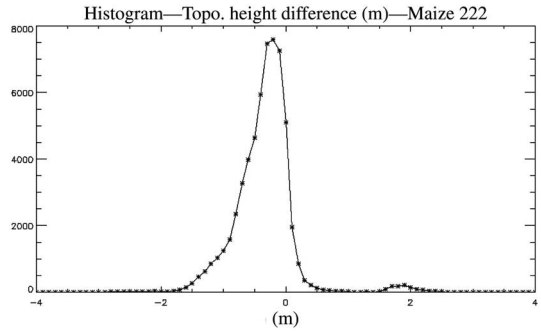

Fig. 8. Histogram for maize from the Agrisar 2006 test site.

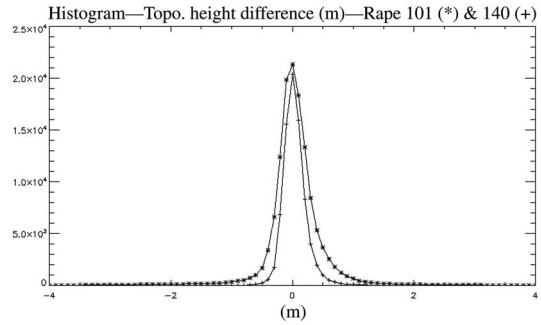

Fig. 9. Histogram for rape from the Agrisar 2006 test site.

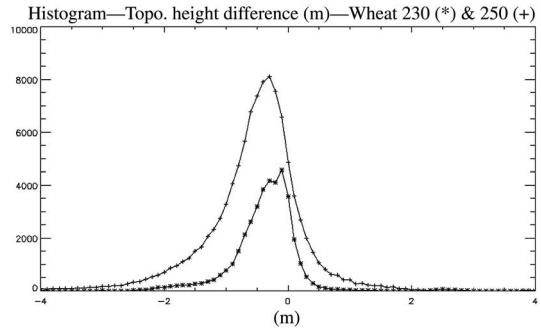

Fig. 10. Histogram for wheat from the Agrisar 2006 test site.

In any case, the bias seems to be an appropriate criterion for setting the threshold for the subsequent computation of the map displaying the test output. Therefore, a 0.25-m threshold will be used for this data set. It must be highlighted that these observations are consistent with the analysis and results in [23], where the linear arrangement of coherences was clearly observed for rape fields but it was not so evident for maize and wheat. Actually, the variation coefficient (i.e., the ratio between the standard deviation and the mean value) of height estimates for rape was clearly lower than for maize and wheat (see Table I in [23]).

To further support the results and the interpretation provided so far, we have also computed 2-D scatter plots relating the retrieved crop height to the topographic phase difference, shown in Figs. 12–14. These results are consistent with the previous analysis since it is the rape field 140 the one which exhibits the narrowest distribution of points, which is also centered around the height crop reported in the ground-truth campaign (see Table I). As expected, the 2-D distributions for

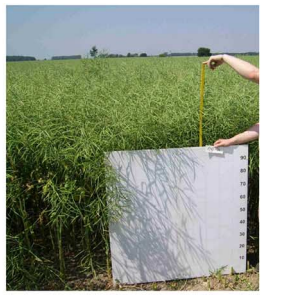

Rape 140

Maize 222

Wheat 250

Fig. 11. Photographs of the three crop types of AgriSAR 2006 campaign on the date of acquisition (July 5, 2006).

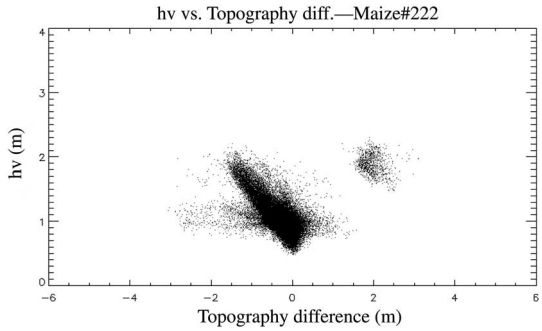

Fig. 12. Maize height versus topographic difference for the Agrisar 2006 test site. The ROI is the one indicated in Fig. 7.

maize and wheat 230 confirm the bias that was found in the 1-D histograms, and the rape and wheat parcels 101 and 250, respectively, display the highest variability as shown previously.

According to the previous analysis a binary map has been computed for characterizing the fields as RVoG or non-RVoG, as displayed in Fig. 15, where black means that RVoG is fulfilled and white relates to non-RVoG pixels. As shown, from the statistical point of view the rape fields are well modeled by means of the RVoG whereas maize and wheat exhibit more variation. The reasons for this difference are two: 1) The lower

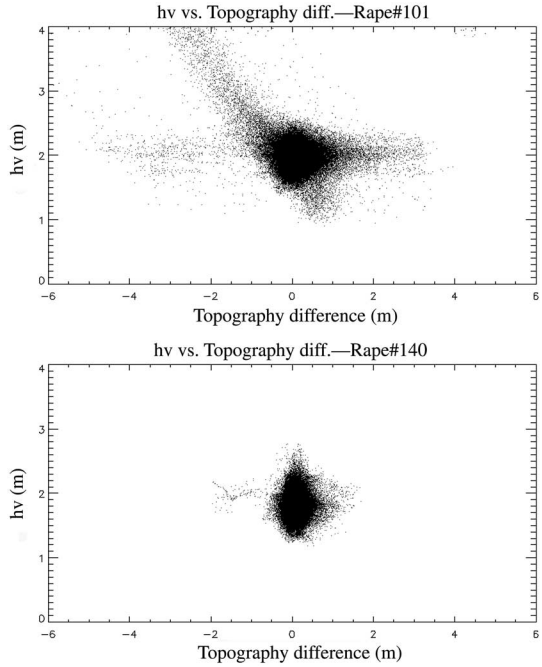

Fig. 13. Rape height versus topographic difference for the Agrisar 2006 test site. The ROI is the one indicated in Fig. 7.

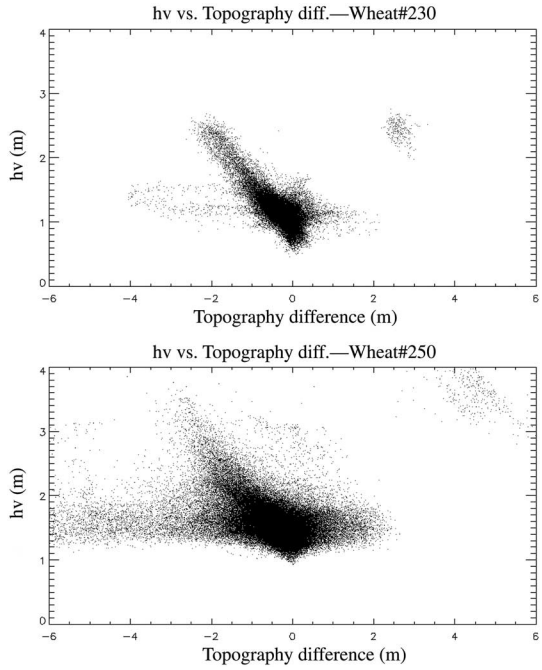

Fig. 14. Wheat height versus topographic difference for the Agrisar 2006 test site. The ROI is the one indicated in Fig. 7.

sensitivity (i.e., lower $k_z \cdot h_v$) within maize and wheat fields due to their lower heights (roughly 1 m) at the time of data acquisition, and 2) The different morphologies characterizing all three crops and heterogeneities inside a particular crop. Reason 1 becomes evident in rape fields since at far-range there is a wider area colored in white from pixel 900 onwards, that is to say, the RVoG is not valid anymore because of a lack of sensitivity (higher incidence and, hence, lower k_z). On the other hand, both reasons 1 and 2 can influence the results in maize and wheat where both dominant black and white areas are present depending on the location within the parcel. Note also that the lack of interferometric sensitivity is the primary reason explaining the results in the wheat field 250 at far-range.

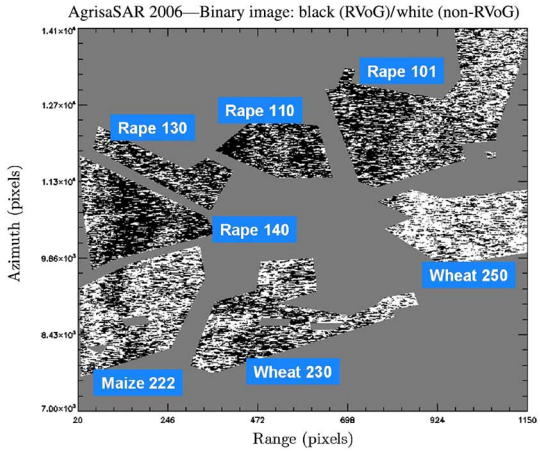

Fig. 15. Binary map for Agrisar 2006 test site. Black pixels fulfil the RVoG and white pixels do not.

It is also important to point out that the output RVoG/Non-RVoG masks and the subsequent final results of the height retrieval (or other parameters) should still be checked for consistency even if the RVoG test is passed. This step would be necessary to prevent wrong conclusions in the event of an unexpected non-RVoG Ω_{12} matrix producing the same results as if its structure was that of a RVoG. This potential failure of the algorithm deserves further investigation and, as the algorithm stands now, it should be used as a sort of "supervised" algorithm no matter the output of the test.

2) Forest: We have also applied the proposed algorithm to a tropical forest scenario. It corresponds to the Mawas test site, located in central Kalimantan, Indonesia, as a part of the INDREX-II campaign funded by ESA in 2004. SAR data acquisitions were conducted by DLR's E-SAR system. The test site corresponds to a peat-swamp forest ranging from 5 to 27 m over a perfectly flat terrain at 6 m AMSL where slopes are less than 0.1% with dimensions 3 km $\times$ 15 km. The algorithm is tested at P-band with a 15-m baseline.

Fig. 16 displays the topography values retrieved by the line fitting method (left) and the one from (1) (right). It is noted that the line fitting approach proposed in [49] was used for this data set since it has been proven to be more robust than the classical least squares estimation. At the top, a river is present and the surrounding area is covered by secondary short vegetation up to 2 m high.

As observed, there are clear differences between both methods which are even more noticeable at far-range (located at the right of the maps). Also, note the noisy estimates along the river due to the low coherence. Figure 17 shows the difference map which suggests that the RVoG is fulfilled in some areas at near-range (more green color) but it fails to model the target within wide areas at middle and far-range. Histograms corresponding to the pixels contained within pink boxes have been computed and shown in Fig. 18. On one hand, the histogram for

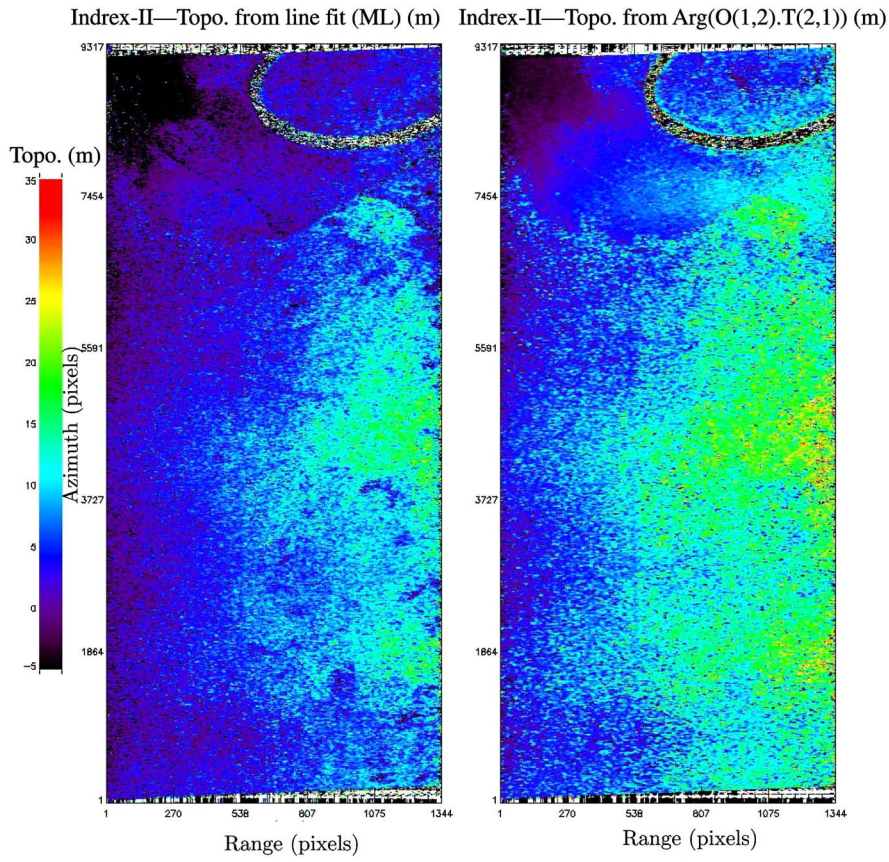

Fig. 16. Topography estimates from (left) line fitting proposed in [49] and (right) (1) proposed in [40].

near-range has a mean value slightly higher than 2.5 m. This fact confirms that the alternative criterion for setting the threshold as a function of volume height would also be a reasonable choice (whenever the height were known) since it corresponds to a 10% of a 25-m tall forest. On the other hand, the histogram for far-range demonstrates that the RVoG would not be valid at that area for this data set because of the high standard deviation. Finally, the RVoG/non-RVoG map for this test site is also generated and displayed in Figure 19, where the same conclusions on the range-dependent validity of the model can be drawn. In addition, the river pixels do not fulfill the RVoG assumption since noise is dominant and the low vegetation areas (peat swamp, see also RGB images in [50]) surrounding the river appear also as non-RVoG zones, since the low volume is almost transparent to P-band signals and the response is mostly made up by ground returns. It is noted that on such areas the topography estimation by the line fitting approach yields correct values due to the high coherence present on them. However, the (1,2) element of the polarimetric interferometric coherency matrix provides biased estimates specially at middle- and far-range. As stated in the previous section, there are two different reasons that could affect the validity of the RVoG. On one hand, the variation of sensitivity of the interferometer along range dimension and, on the other hand, the potential different morphologies of the vegetation. According to the configuration of the sensor at middle-range the vertical wavenumber was less than 0.06. Although at higher incidences the sensor is expected to be more sensitive to the volume (the wave travels a longer path through the volume), these κ_z values are in the limit to ensure enough sensitivity for a correct parameter retrieval. This was also stated in [9], where the forest height retrieval was carried out by using a multibaseline approach, using a total of four baselines for an optimum height estimation. As shown in Fig. 20, a transect covering the whole range dimension has been considered and the corresponding phase signatures have been plotted. A slight disagreement between both estimates is present; however, when transforming the phase to height values important differences appear, as shown in the histograms in Fig. 21. The line fitting approach performs quite well for the whole transect along the range dimension and this is because the sensor maps sufficiently well the ground and this leads to correctly retrieve the topographic phase. However, the $Arg(O(1,2)T(2,1))$ height exhibits more variability and this would suggest that in the particular case of the tropical forest in Mawas-E test site there appear different propagation effects inducing additional terms in the $Arg(O(1,2)T(2,1))$ phase. As seen, the topographic height by the line fitting exhibits a small bias around 1 m whereas the phase from element (1,2) reveals a wider height distribution. According to [50], this is a peat swamp area; therefore, it is plausible that low and nonuniform vegetation could induce phase variations on (1,2) element. Nevertheless, this issue must be further investigated

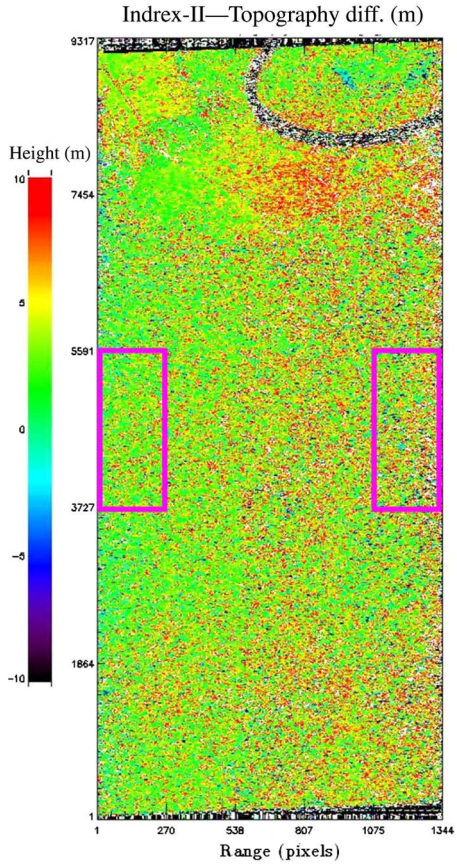

Fig. 17. Phase difference map for INDREX-II test site.

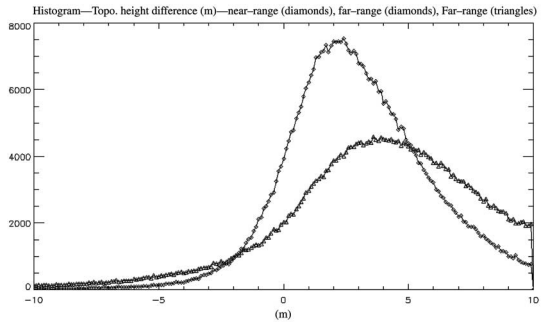

Fig. 18. Histograms of phase difference at near- and far-range for INDREX-II test site.

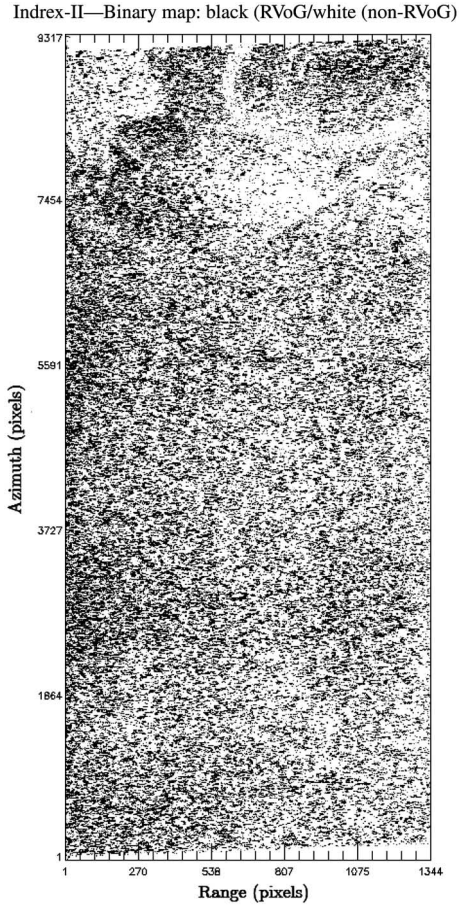

Fig. 19. Binary map for INDREX-II test site. Black pixels fulfil the RVoG and white pixels do not.

and confirmed. In addition, we must point out that far-range areas for this data set are characterized by a low sensitivity, so the RVoG/non-RVoG discrimination could be affected by this issue.

At this stage, some remarks on the possible causes that lead the RVoG assumptions to break down are given. On one hand, speckle noise has been minimized by performing a 15 $\times$ 15 multilook on both airborne data sets. Despite this averaging, residual noise could be affecting the subsequent phase estimates. This could be a limiting factor specially in the $\arg(\Omega_{12}(1,2)T(2,1))$ value since the magnitude of the correlation between both matrix elements (i.e. $|\Omega_{12}(1,2)T(2,1)|$) is low. This means that an unbiased estimation would require a higher number of samples. Such an issue has not been studied in this paper and requires further investigation.

Second, the interaction of factors related to the vegetation structure and sensor configuration (i.e. vertical wavenumber) must also be taken into account. There are three cases to consider: 1) volume decorrelation and the size of the particles becoming much larger than the wavelength; 2) the incidence angle increases and, hence, the κ_z gets lower so the sensor provides a lower sensitivity; and 3) a heterogeneous morphology of the vegetation which induces anisotropic wave propagation. From the results presented in this paper, case 1) is the cause of RVoG failure for indoor data. For the agricultural site, case 2) provokes a higher amount of non-RVoG pixels at far-range for the rape field. For lower vegetation (i.e., heights from 77 cm to 1.1 m), cases 2) and 3) can both contribute to the RVoG failure, even though a more precise explanation on this issue cannot be given. On the other hand, it seems evident that case 2) is the primary source of failure of RVoG assumptions according to the low vertical wavenumber which is lower than 0.06 from mid- to far-range. Nevertheless, note that this fact can be also compatible with potential orientation effects occurring due to the long wavelength at P-band [39].

Finally, one key limiting factor in repeat-pass PolInSAR is temporal decorrelation. The impact of such an issue has been addressed in a number of studies related to the PolInSAR/RVoG paradigm [51], [52]. It has been shown that wind-induced

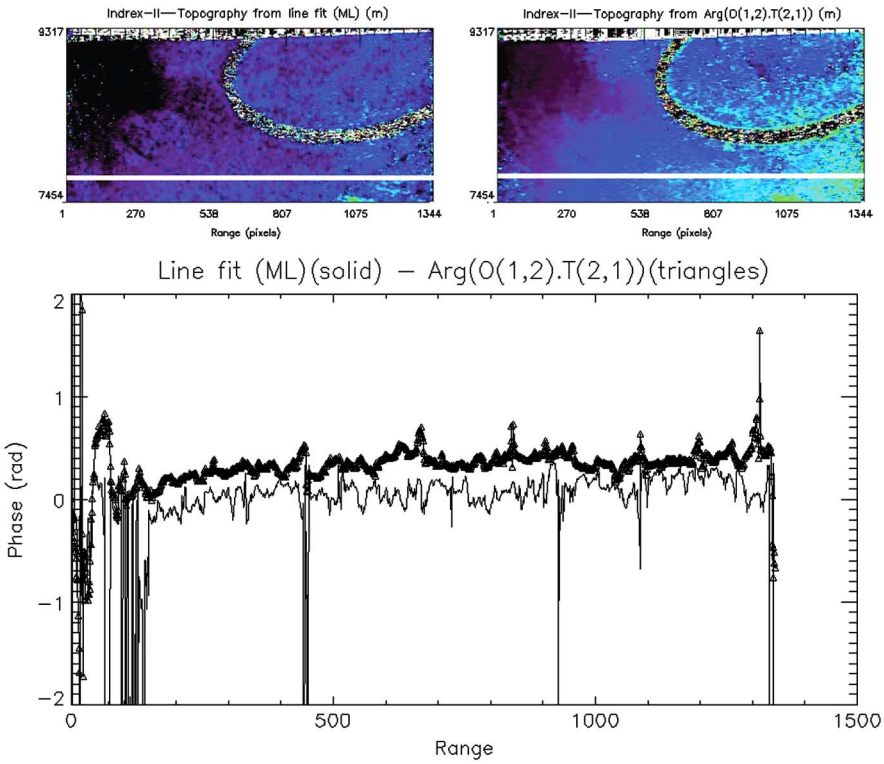

Fig. 20. Transect (white) for INDREX-II test site and the corresponding plots of topographic phase for both methods.

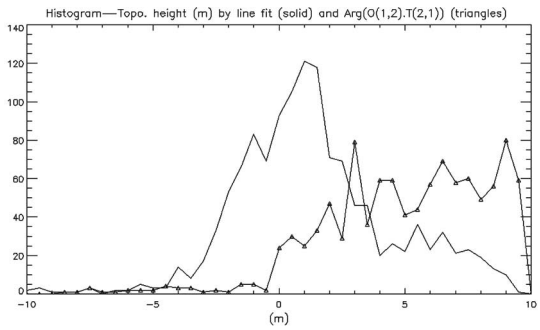

Fig. 21. Histograms of topographic height for both methods for the selected transect.

motion and dielectric changes of vegetation and ground severely bias the retrieved parameters. In particular, wind-induced decorrelation is the critical factor for short-term (i.e., order of minutes) repeat-pass PolInSAR. In case of airborne data sets employed in this study, temporal baselines were 21.5 and 20 min for AgriSAR and INDREX-II, respectively, and no windy conditions were reported during those acquisition intervals, so it is expected that temporal decorrelation is not an issue in these cases. Note, however, that the proposed algorithm does not consider temporal decorrelation so its application is limited to single-pass or short-term repeat-pass PolInSAR.

IV. Conclusion

A simple algorithm for discrimination between RVoG and non-RVoG areas has been proposed in this paper. The algorithm is based on two different methods proposed in the literature for retrieving the topographic phase, i.e., the line fitting approach and the observation of the $(1, 2)$ element of the polarimetric interferometric coherency matrix. Since both concepts stem from the random volume over ground assumptions, it is expected that topography estimates retrieved from them are very similar in case of a vegetated scene fulfilling the RVoG hypothesis. On the contrary, different topographic values are explained as a violation of the RVoG assumptions. This interpretation is theoretically supported by means of Freeman–Durden decomposition concept extended to PolInSAR observables. The construction of such a model is based on the same principle commonly applied within the PolInSAR paradigm regarding the addition of uncorrelated contributions of first-order scattering mechanisms. The algorithm requires a histogram analysis in order to derive the appropriate threshold to decide whether both topography estimates are similar or not. Three different data sets (indoor and air-borne data) over agricultural and tropical forest scenarios have been analyzed. According to the histogram analysis, the corresponding thresholds for RVoG discrimination on agricultural and forest areas are about 25 cm and 2.5 m, respectively, which is consistent with topography estimation errors reported in previous studies. However, a more accurate vegetation parameter estimation would require a local assessment of the RVoG validity. This can be implemented by computing histograms for a fixed area (e.g., 10×10 pixels) and setting the threshold in an adaptive way. Nevertheless, other alternative strategies could possibly lead to an improvement on the threshold selection. On one hand, parametric and nonparametric statistical tests are also being considered. On the other hand, the joint use of the vertical wavenumber (i.e., sensitivity) and the Cramer–Rao lower

bound of the topographic phase (which could be obtained as for the volume height in [53]) would provide the expected maximum deviation from the true topographic value. For a practical application, it is noted that the proposed RVoG/Non-RVoG test must be used as a supervised tool no matter the output of the procedure. Hence, the output RVoG/non-RVoG masks and the subsequent final results of the height retrieval (or other parameters) should still be checked for consistency even if the RVoG test is passed. This step would be necessary to prevent wrong conclusions in the event of an unexpected non-RVoG Ω_{12} matrix producing the same results as if its structure was that of an RVoG. Finally, the proposed algorithm does not consider temporal decorrelation so its application is limited to single-pass or short-term repeat-pass PolInSAR.

ACKNOWLEDGMENT

The authors would like to thank Prof. I. Hajnsek (DLR) for kindly providing access to the interferometric data acquired in parallel to the AgriSAR2006 campaign. They are also grateful to the anonymous reviewers for their constructive comments which helped us to improve the paper.

REFERENCES

[1] R. N. Treuhaft, S. N. Madsen, M. Moghaddam, and J. J. van Zyl, "Vegetation characteristics and underlying topography from interferometric radar," *Radio Sci.*, vol. 31, no. 6, pp. 1449–1485, Nov. 1996.

[2] R. N. Treuhaft and S. R. Cloude, "The structure of oriented vegetation from polarimetric interferometry," *IEEE Trans. Geosci. Remote Sens.*, vol. 37, no. 5, pp. 2620–2624, Sep. 1999.

[3] R. N. Treuhaft and P. R. Siqueira, "Vertical structure of vegetated land surfaces from interferometric and polarimetric data," *Radio Sci.*, vol. 35, pp. 141–177, 2000.

[4] S. R. Cloude and K. P. Papathanassiou, "Polarimetric SAR interferometry," *IEEE Trans. Geosci. Remote Sens.*, vol. 36, no. 5, pp. 1551–1565, Sep. 1998.

[5] K. P. Papathanassiou and S. R. Cloude, "Single baseline polarimetric SAR interferometry," *IEEE Trans. Geosci. Remote Sens.*, vol. 39, no. 11, pp. 2352–2363, Nov. 2001.

[6] S. R. Cloude and K. P. Papathanassiou, "Three-stage inversion process for polarimetric SAR interferometry," *IEE Proc. Radar Sonar Navigat.*, vol. 150, no. 3, pp. 125–134, Jun. 2003.

[7] T. Mette, K. P. Papathanassiou, and I. Hajnsek, "Applying a common allometric equation to convert forest height from pol-inSAR data to forest biomass," in *Proc. IEEE Int. Geosci. Remote Sens. Symp. (IGARSS)*, Anchorage, AK, USA, Sep. 2004, p. 272.

[8] T. Mette, K. P. Papathanassiou, and I. Hajnsek, "Biomass estimation from polarimetric SAR interferometry over heterogeneous forest terrain," in *Proc. IEEE Int. Geosci. Remote Sens. Symp. (IGARSS)*, Anchorage, AK, USA, Sep. 2004.

[9] I. Hajnsek, F. Kugler, L. Seung-Kuk, and K. P. Papathanassiou, "Tropical-forest-parameter estimation by means of pol-InSAR: The INDREX-II campaign," *IEEE Trans. Geosci. Remote Sens.*, vol. 47, no. 2, pp. 481–493, Feb. 2009.

[10] J. Praks, F. Kugler, K. P. Papathanassiou, I. Hajnsek, and M. Hallikainen, "Height estimation of boreal forest: Interferometric model-based inversion at l- and x-Band versus HUTSCAT profiling scatterometer," *IEEE Geosci. Remote Sens. Lett.*, vol. 4, no. 3, pp. 466–470, Jul. 2007.

[11] M. Neumann, L. Ferro-Famil, and A. Reigber, "Estimation of forest structure, ground, and canopy layer characteristics from multibaseline polarimetric interferometric SAR data," *IEEE Trans. Geosci. Remote Sens.*, vol. 48, no. 3, pp. 1086–1104, Mar. 2010.

[12] F. Garestier, P. C. Dubois-Fernandez, and K. P. Papathanassiou, "Pine forest height inversion using single-pass x-Band PolInSAR data," *IEEE Trans. Geosci. Remote Sens.*, vol. 46, no. 11, pp. 3544–3559, Jan. 2008.

[13] F. Garestier, P. C. Dubois-Fernandez, and I. Champion, "Forest height inversion using high-resolution p-band pol-InSAR data," *IEEE Trans. Geosci. Remote Sens.*, vol. 46, no. 1, pp. 59–68, Nov. 2008.

[14] A. Reigber and A. Moreira, "First demonstration of airborne SAR tomography using multibaseline L-band data," *IEEE Trans. Geosci. Remote Sens.*, vol. 38, no. 5, pp. 2142–2152, Sep. 2000.

[15] S. R. Cloude, "Polarisation coherence tomography," *Radio Sci.*, vol. 41, Apr. 2006.

[16] S. R. Cloude, "Dual baseline coherence tomography," *IEEE Geosci. Remote Sens. Lett.*, vol. 4, no. 1, pp. 127–131, Jan. 2007.

[17] S. Tebaldini, "Algebraic synthesis of forest scenarios from multibaseline PolInSAR data," *IEEE Trans. Geosci. Remote Sens.*, vol. 47, no. 12, pp. 4132–4142, 2009.

[18] S. Tebaldini and F. Rocca, "Multibaseline polarimetric SAR tomography of a boreal forest at p- and l-bands," *IEEE Trans. Geosci. Remote Sens.*, vol. 50, no. 1, pp. 232–246, Jan. 2012.

[19] L. Ferro-Famil and S. Tebaldini, "Maximum likelihood SAR tomography based on the polarimetric multi-baseline RVoG model: Optimal estimation of a covariance matrix structured as the sum of two kronecker products," in *Proc. 6th POLinSAR Workshop*, Frascati, Italy, Jan. 2013 [CD-ROM].

[20] I. Hajnsek and S. R. Cloude, "Pol-inSAR for agricultural vegetation parameter estimation," in *Proc. IEEE Int. Geosci. Remote Sens. Symp. (IGARSS)*, Anchorage, AK, USA, Sep. 2004, pp. 1224–1227.

[21] J. D. Ballester-Berman, J. M. Lopez-Sanchez, and J. Fortuny-Guasch, "Retrieval of biophysical parameters of agricultural crops using polarimetric SAR interferometry," *IEEE Trans. Geosci. Remote Sens.*, vol. 43, no. 4, pp. 683–694, Apr. 2005.

[22] J. M. Lopez-Sanchez, J. D. Ballester-Berman, and J. Fortuny-Guasch, "Indoor wide-band polarimetric measurements on maize plants: A study of the differential extinction coefficient," *IEEE Trans. Geosci. Remote Sens.*, vol. 44, no. 4, pp. 758–767, Apr. 2006.

[23] J. M. Lopez-Sanchez, I. Hajnsek, and J. D. Ballester-Berman, "First demonstration of agriculture height retrieval with PolInSAR airborne data," *IEEE Geosci. Remote Sens. Lett.*, vol. 9, no. 2, pp. 242–246, Mar. 2012.

[24] A. Freeman and S. L. Durden, "A three component scattering model to describe polarimetric SAR data," in *Proc. SPIE Radar Polarimetry*, 1992, vol. 1748, pp. 213–224.

[25] A. Freeman and S. L. Durden, "A three-component scattering model for polarimetric SAR data," *IEEE Trans. Geosci. Remote Sens.*, vol. 36, no. 3, pp. 963–973, May 1998.

[26] Y. Yamaguchi, T. Moriyama, M. Ishido, and H. Yamada, "Four-component scattering model for polarimetric SAR image decomposition," *IEEE Trans. Geosci. Remote Sens.*, vol. 43, no. 8, pp. 1699–1706, Aug. 2005.

[27] Y. Yamaguchi, A. Sato, W. M. Boerner, R. Sato, and H. Yamada, "Four-component scattering power decomposition with rotation of coherency matrix," *IEEE Trans. Geosci. Remote Sens.*, vol. 49, no. 6, pp. 2251–2258, Jun. 2011.

[28] J. J. Van Zyl, M. Arii, and Y. Kim, "Model-based decomposition of polarimetric SAR covariance matrices constrained for nonnegative eigenvalues," *IEEE Trans. Geosci. Remote Sens.*, vol. 49, no. 9, pp. 3452–3459, Sep. 2011.

[29] Y. Cui *et al.*, "On complete model-based decomposition of polarimetric SAR coherency matrix data," *IEEE Trans. Geosci. Remote Sens.*, vol. 52, no. 4, pp. 1991–2001, Apr. 2014.

[30] J.-S. Lee, T. L. Ainsworth, and Y. Wang, "Generalized polarimetric model-based decompositions using incoherent scattering models," *IEEE Trans. Geosci. Remote Sens.*, vol. 52, no. 5, pp. 2474–2491, May 2014.

[31] S. W. Chen, X. S. Wang, S. P. Xiao, and M. Sato, "General polarimetric model-based decomposition for coherency matrix," *IEEE Trans. Geosci. Remote Sens.*, vol. 52, no. 3, pp. 1843–1855, Mar. 2014.

[32] S. W. Chen, X. S. Wang, Y. Z. Li, and M. Sato, "Adaptive model-based polarimetric decomposition using polInSAR coherence," *IEEE Trans. Geosci. Remote Sens.*, vol. 52, no. 3, pp. 1705–1718, Mar. 2014.

[33] S. W. Chen, Y.-Z. Li, X.-S. Wang, S.-P. Xiao, and M. Sato, "Modeling and interpretation of scattering mechanisms in polarimetric SAR: Advances and perspectives," *IEEE Signal Process. Mag.*, vol. 31, no. 4, pp. 79–89, Jul. 2014.

[34] J. D. Ballester-Berman and J. M. Lopez-Sanchez, "Applying the Freeman–Durden decomposition concept to polarimetric SAR interferometry," *IEEE Trans. Geosci. Remote Sens.*, vol. 48, no. 1, pp. 466–479, Jan. 2010.

[35] L. Ferro-Famil and M. Neumann, "Recent advances in the derivation of POL-inSAR statistics: Study and applications," in *Proc. 7th Eur. Conf. Synth. Aperture Radar (EUSAR)*, Friedrichshafen, Germany, Jun. 2008, pp. 1–4.

[36] K. Conradsen, A. A. Nielsen, J. Schou, and H. Skriver, "A test statistic in the complex wishart distribution and its application to change detection in polarimetric SAR data," *IEEE Trans. Geosci. Remote Sens.*, vol. 41, no. 1, pp. 4–19, Jan. 2003.

[37] A. Marino, S. R. Cloude, and J. M. Lopez-Sanchez, "Test of equi-scattering mechanisms for POLInSAR applications with tanDEM-X," in *Proc. IEEE Int. Geosci. Remote Sens. Symp. (IGARSS)*, Vancouver, BC, Canada, Jul. 2011, pp. 2715–2718.

[38] A. Marino, S. R. Cloude, and J. M. Lopez-Sanchez, "A new polarimetric change detector in radar imagery," *IEEE Trans. Geosci. Remote Sens.*, vol. 51, no. 5, pp. 2986–3000, May 2013.

[39] C. Lopez-Martinez and A. Alonso-Gonzalez, "Assessment and estimation of the RVoG model in polarimetric SAR interferometry," *IEEE Trans. Geosci. Remote Sens.*, vol. 52, no. 6, pp. 3091–3106, Jun. 2014.

[40] C. Lopez-Martinez, A. Alonso, X. Fabregas, and K. P. Papathannassiou, "Ground topography estimation over forests considering polarimetric SAR interferometry," in *Proc. IEEE Int. Geosci. Remote Sens. Symp. (IGARSS)*, 2010, pp. 3612–3615.

[41] M. Tabb, T. Flynn, and R. Carande, "Full maximum likelihood inversion of polInSAR scattering models," in *Proc. IEEE Int. Geosci. Remote Sens. Symp. (IGARSS)*, Anchorage, AK, USA, Sep. 2004, pp. 1232–1235.

[42] J. D. Ballester-Berman and J. M. Lopez-Sanchez, "Coherence loci for a homogeneous volume over a double-Bounce ground return," *IEEE Geosci. Remote Sens. Lett.*, vol. 4, no. 2, pp. 317–321, Apr. 2007.

[43] J. D. Ballester-Berman and J. M. Lopez-Sanchez, "Combination of direct and double-Bounce ground responses in the homogeneous oriented volume over ground model," *IEEE Geosci. Remote Sens. Lett.*, vol. 8, no. 1, pp. 54–58, Jan. 2011.

[44] C. Lopez-Martinez and K. P. Papathanassiou, "Cancellation of scattering mechanisms in polInSAR: Application to underlying topography estimation," *IEEE Trans. Geosci. Remote Sens.*, vol. 51, no. 2, pp. 953–965, Feb. 2013.

[45] J. D. Ballester-Berman, J. M. Lopez-Sanchez, and F. Vicente-Guijalba, "Follow-up investigations on model-based PolInSAR techniques," in *Proc. 10th Eur. Conf. Synth. Aperture Radar (EUSAR)*, Berlin, Germany, Jun. 2014, pp. 1–4.

[46] I. Hajnsek *et al.*, "AGRISAR 2006—Agricultural bio-/geophysical retrievals from frequent repeat SAR and optical imaging," European Space Agency (ESA), Final Report. 19974/06/I-LG, 2008.

[47] P. Dubois-Fernandez, A. Arnaubec, and X. Dupuis, "Assessment of single baseline PolInSAR in tropical context for vegetation characterisation," in *Proc. 6th POLinSAR Workshop*, Frascati, Italy, Jan. 2013 [CD-ROM].

[48] F. T. Ulaby, R. K. Moore, and A. K. Fung, *Microwave Remote Sensing: From Theory to Applications*. vol. III, Dedham, MA, USA: Artech House, 1986.

[49] L. Ferro-Famil, M. Neumann, and Y. Huang, "Multi-baseline pol-InSAR statistical techniques for the characterization of distributed media," in *Proc. IEEE Int. Geosci. Remote Sens. Symp. (IGARSS'09)*, 2009, vol. 3, pp. III-971–III-974.

[50] I. Hajnsek *et al.*, *INDREX-II Indonesian Radar Experiment Campaign Over Tropical Forest in L- and P-band*, European Space Agency (ESA), Final Report, 2006.

[51] M. Lavalle, M. Simard, and S. Hensley, "A temporal decorrelation model for polarimetric radar interferometers," *IEEE Trans. Geosci. Remote Sens.*, vol. 50, no. 7, pp. 2880–2888, Jul. 2012.

[52] S.-K. Lee, F. Kugler, K. P. Papathanassiou, and I. Hajnsek, "Quantification of temporal decorrelation effects at l-Band for polarimetric SAR interferometry applications," *IEEE J. Sel. Topics Appl. Earth Observ. Remote Sens.*, vol. 6, no. 3, pp. 1351–1367, Jun. 2013.

[53] A. Roueff, A. Arnaubec, P. C. Dubois-Fernandez, and P. Réfrégier, "Cramer-rao lower bound analysis of vegetation height estimation with random volume over ground model and polarimetric SAR interferometry," *IEEE Geosci. Remote Sens. Lett.*, vol. 8, no. 6, pp. 1115–1119, Nov. 2011.

J. David Ballester-Berman was born in Xixona, Spain. He received the Ing. degree in telecommunications engineering from the Technical University of Valencia, Valencia, Spain, in 2000, and the Dr.Ing. degree in telecommunications engineering from the University of Alicante, Alicante, Spain, in 2007.

From 2000 to 2001, he was a Support Engineer in the development of software tools for the planning and design of terrestrial digital television systems. Since 2001, he has been with the Signals, Systems, and Telecommunication Group, University of Alicante, carrying out educational and research tasks. His research interests include polarimetric synthetic aperture radar interferometry techniques for vegetation monitoring.

Fernando Vicente-Guijalba was born in Elche, Alicante, Spain, in 1981. He received the Ingeniero Tecnico degree in telecommunication engineering and the Ingeniero degree in sound and image engineering from the University of Alicante, in 2006 and 2011, respectively.

Since 2011, he has been a Pre-Doctoral Fellow with the Signals, Systems, and Telecommunications Groups, University of Alicante. His research interests include dynamical systems analysis with applications in the polarimetric and interferometric SAR methods.

Juan M. Lopez-Sanchez (S'94–M'00–SM'05) was born in Alicante, Spain, in 1972. He received the Ingeniero (M.S). and Doctor Ingeniero (Ph.D.) degrees in telecommunication engineering from the Technical University of Valencia (UPV), Valencia, Spain, in 1996 and 2000, respectively.

From 1998 to 1999, he worked as a Pre-Doctoral Grantholder with the Space Applications Institute, Joint Research Centre of the European Commission, Ispra, Italy. Since 2000, he leads the Signals, Systems, and Telecommunication Group, University of Alicante, Alicante, Spain, where he is a Full Professor since November 2011. He has coauthored more than 50 papers in refereed journals and more than 90 papers and presentations in international conferences and symposia. His research interests include microwave remote sensing for inversion of biophysical parameters, polarimetric and interferometric techniques, SAR imaging algorithms, and analytical and numerical models for multiple scattering problems.

Dr. Lopez-Sanchez was the Chair of the Spanish Chapter of the IEEE Geoscience and Remote Sensing Society from 2006 to 2012. In 2001, he was the recipient of the Indra Award for the best Ph.D. thesis about radar in Spain.